Solubility of U(VI) in chloride solutions. II. The stable oxides/hydroxides in alkaline KCl solutions: Thermodynamic description and relevance in cementitious systems

Neşe Çevirim-Papaioannou[a,*], Ezgi Yalçıntaş[a,b], Xavier Gaona[a,**], Marcus Altmaier[a], Horst Geckeis[a]

[a] Karlsruhe Institute of Technology, Institute for Nuclear Waste Disposal, P.O. Box 3640, 76021, Karlsruhe, Germany
[b] Los Alamos National Laboratory, Carlsbad, NM, 88220, USA

ARTICLE INFO

Keywords:
Uranium
U(VI)
Solubility
Hydrolysis
KCl
Thermodynamics
SIT
Cement

ABSTRACT

The solubility of U(VI) is investigated from undersaturation conditions in 0.1, 0.51, 1.03, 3.31 and 4.58 m KCl–KOH solutions at pH_m = 7.5–14.6 (with pH_m = –log [H^+] in molal units). All experiments were performed under Ar atmosphere at T = (22 ± 2)°C. XRD, quantitative chemical analysis, SEM–EDS and TG–DTA confirm that $K_2U_2O_7{\cdot}1.5H_2O$(cr) is the solid phase controlling the solubility in all evaluated systems at $pH_m \geq 9.5$. Below this pH_m and with decreasing KCl concentration, the formation of sub-stoichiometric phases with K:U < 1 is indicated by XRD and solubility data. The concentration of uranium in equilibrium with $K_2U_2O_7{\cdot}1.5H_2O$(cr) shows a pH-independent behaviour up to $pH_m \approx 11$ regardless of ionic strength, whereas an increase of the solubility with a well–defined slope of +1 (log [U] *vs.* pH_m) is observed at $pH_m \geq 11$. These results are consistent with the predominance of $UO_2(OH)_3^-$ and $UO_2(OH)_4^{2-}$ species as previously reported in the literature. The combination of solubility data obtained in the present study with $K_2U_2O_7{\cdot}1.5H_2O$(cr) and the U(VI) hydrolysis scheme reported in Altmaier et al. (2017) yields a solubility product of log ${}^*K^\circ_{s,0}\{0.5K_2U_2O_7{\cdot}1.5H_2O(cr)\}$ = (12.0 ± 0.2). SIT ion interaction coefficients for $UO_2(OH)_3^-$ and $UO_2(OH)_4^{2-}$ with K^+ are derived based on the newly generated experimental data in dilute to concentrated KCl systems and analogy with NaCl systems. This work extends the thermodynamic database available for U(VI) and allows more accurate source term calculations in the context of nuclear waste disposal under boundary conditions where significant K concentrations may be present and redox conditions lie in the stability field of U(VI). The $K_2U_2O_7{\cdot}1.5H_2O$(cr) solid phase can be considered to control the solubility of U(VI) in the degradation phase I of cement and cementitious materials.

1. Introduction

Potassium is the second most abundant alkali metal in the Earth crust (2.35%), only slightly behind sodium (2.40%). Accordingly, potassium is also an abundant cation in surface- and groundwaters. In the context of repositories for nuclear waste, large inventories of potassium are found in cementitious materials used for the stabilization of the waste and several construction purposes (up to 4% of the total mass, as K_2O in unaltered pastes) (Berner, 1992; Taylor, 1997; Wieland and Van Loon, 2003). In salt-rock formations considered/used as disposal sites (e.g. El Salado Formation in WIPP – Yamazaki et al., 1992; Snider, 2003; Lucchini et al., 2007) as well as in other geological formations located in the vicinity of rock-salt formations (e.g. sedimentary bedrocks in the Canadian Shield and Cretaceous argillites in Northern Germany (Brewitz, 1980; Frape et al., 1984; Duro et al., 2010)) potassium likewise can be present in significant concentrations (up to ≈ 0.8 M).

A number of minerals containing potassium and uranium were described in the literature, highlighting the stability of K–U compounds under a variety of geochemical conditions: clarkeite $(Na,K)_{2-2x}(Ca,Pb)_xU_2O_7{\cdot}yH_2O$(cr), compreignacite ($K_2U_6O_{19}{\cdot}11H_2O$(cr), agrinierite $K_2(Ca_{0.65}Sr_{0.35})[(UO_2)_3O_3(OH)_2]_2{\cdot}5H_2O$(cr), abernathyite ($K_2(UO_2)_2(AsO_4)_2{\cdot}8H_2O$(cr)), carnotite ($K_2(UO_2)_2(VO_4)_2{\cdot}nH_2O$(cr)), zippeite ($K_4(UO_2)_6(SO_4)_3(OH)_{10}{\cdot}4H_2O$(cr)), meta-ankoleite $KUO_2PO_4{\cdot}4H_2O$(cr), K-autunite ($K(UO_2)(PO_4)$(cr)), grimselite ($NaK_3UO_2(CO_3)_3{\cdot}H_2O$(cr)), boltwoodite ($K(UO_2)(SiO_3OH){\cdot}H_2O$(cr)),

* Corresponding author.
** Corresponding author.
E-mail addresses: nese.cevirim@kit.edu (N. Çevirim-Papaioannou), xavier.gaona@kit.edu (X. Gaona).

among others (Frondel and Fleischer, 1954; Grenthe et al., 1992, 2006; Gorman-Lewis et al., 2008a,b). Within the ternary system K–U(VI)–O, the Thermochemical Database project of the Nuclear Energy Agency (NEA–TDB) selected thermodynamic data for four different compounds, namely KUO_4(cr), $K_2U_2O_7$(cr), $K_2U_4O_{13}$(cr) and $K_2U_6O_{19}{\cdot}11H_2O$(cr) (Grenthe et al., 1992; Guillaumont et al., 2003). Most of the thermodynamic data selection for this system is based upon thermochemical studies with very crystalline solid phases synthesized at high temperatures, which are highly questionable as solubility limiting solid phases when modelling uranium solubility control in repository relevant aqueous systems. Only two solubility studies reporting thermodynamic data for this system are available so far in the literature, both dedicated to $K_2U_6O_{19}{\cdot}11H_2O$(cr) (Sandino and Grambow, 1994; Gorman-Lewis et al., 2008b). The solubility study by Yamazaki et al. (1992) reports the formation of $K_2U_2O_7$(s) in concentrated brines, but does not provide thermodynamic data for this compound. A short summary of the main experimental studies investigating the ternary system K–U(VI)–O is provided in the following.

O'Hare and Hoekstra (1974) synthesized K_2UO_4(cr) by reacting U_3O_8 with K_2CO_3 at $T = 1100$ K, and determined the standard enthalpy of formation using calorimetry. Fuger (1985) obtained $K_2U_2O_7$(cr) by reacting stoichiometric mixtures of UO_3 and K metal at high temperature.[1] Based upon calorimetric measurements, the author reported the enthalpy of solution of $K_2U_2O_7$(cr) in 1.0 M HCl. Iyer et al. (1997) investigated the thermodynamic properties of $K_2U_4O_{13}$(cr) and $K_2U_4O_{12}$(cr) by drop calorimetric measurements. The original experimental data were re-evaluated by the NEA–TDB reviewers (Guillaumont et al., 2003), who observed that the heat capacity calculated for $K_2U_4O_{13}$(cr) was not consistent with the general behaviour of the heat capacities of the alkali-metal uranates. Guillaumont and co-workers accordingly did not select thermodynamic data for this compound.

The solubility of $K_2U_6O_{19}{\cdot}11H_2O$(cr) was studied at 25 °C by Sandino and Grambow (1994) and Gorman-Lewis et al. (2008b). Two initial solid phases were used by Sandino and Grambow: (i) $K_2U_6O_{19}{\cdot}11H_2O$(cr) synthesized by reacting stoichiometric amounts of KOH with $UO_2(NO_3)_2$ (first at room temperature, then at $T = 60$ °C for a month, run K1), and (ii) $UO_3{\cdot}2H_2O$(cr) (run K2). Solubility experiments using these solid phases were performed in 1 m KCl solutions at $3.5 \leq pH \leq 5$. After 3 months of contact time, solid phases collected from both series were identified as $K_2U_6O_{19}{\cdot}11H_2O$(cr) using x-ray diffraction (XRD) and scanning electron microscopy – energy dispersive x-ray (SEM–EDX). Solubility constants extrapolated to $I = 0$ were reported as $\log {}^*K^\circ_{s,0}$(run K1) = (38.19 ± 0.23) and $\log {}^*K^\circ_{s,0}$(run K2) = (40.53 ± 0.21) for the equilibrium reaction $K_2U_6O_{19}{\cdot}11H_2O$(cr) + 14 $H^+ \Leftrightarrow$ 2 K^+ + 6 UO_2^{2+} + 18 H_2O(l). The authors attributed the discrepancies between both $\log {}^*K^\circ_{s,0}$ to the different crystallinity of the solid phases. The NEA–TDB re-evaluated the data in Sandino and Grambow (1994) obtaining lower solubility constants, and selected $\log {}^*K^\circ_{s,0}$ = (37.1 ± 0.5) as unweighted average of the K1 and K2 runs (Guillaumont et al., 2003). Gorman-Lewis et al. (2008b) studied the solubility of compreignacite (as $K_2(UO_2)_6O_4(H_2O)_7$) under weakly acidic conditions at $4.3 \leq pH \leq 4.6$. The starting material was synthesized by reacting $UO_2(CH_3COO)_2(H_2O)_2$ with K_2CO_3 in a Teflon vial at pH = 5 and $T = 373$ K during 24 h. Solid phase characterization by XRD, fourier-transform infrared spectroscopy (FT–IR), thermogravimetric analysis (TGA) and chemical analysis confirmed the presence of compreignacite before and after solubility experiments, although a decrease in the degree of crystallinity was observed in the solid phases collected after the solubility experiments. The authors reported $\log {}^*K^\circ_{s,0}$ = (40.5–1.4/+0.2), in agreement with $\log {}^*K^\circ_{s,0}$ of the less crystalline phase (run K2) reported by Sandino and Grambow (1994). Yamazaki et al. (1992) studied the solubility of U(VI) from oversaturation (with $UO_2(NO_3)_2$) and undersaturation conditions. Experiments were performed at $6.4 \leq pH_c \leq 12.4$ (with $pH_c = -\log [H^+]$ in molar units) in a synthetic brine representative of the Waste Isolation Pilot Plant (WIPP) in Carlsbad (New Mexico, USA) containing 1.71 M NaCl, 0.767 M KCl, 1.44 M $MgCl_2$, 0.044 M Na_2SO_4, 0.011 M $NaHCO_3$, 0.005 M NaBr and 0.015 M $CaCl_2$. After attaining equilibrium conditions, two solid phases were identified by XRD: $UO_3{\cdot}2H_2O$(cr) and $K_2U_2O_7$(cr) at $pH_c = 8.4$ and 10.4, respectively. We note that a massive amount of hydroxide (as NaOH) was required in the solubility experiments above $pH_c \approx 9$ to overcome the precipitation of $Mg(OH)_2$(s) or similar solid Mg-phases. Because of the complexity of the synthetic brine used and the ill-defined composition in the solubility experiments above $pH_c \approx 9$, these data cannot be used to derive any thermodynamic quantity of the system under evaluation.

In addition to these thermodynamic studies, a number of publications are dedicated to the structural characterization of K–U(VI)–O compounds. Van Egmond and Cordfunke (1976) investigated the crystal structure of potassium uranate phases with K/U atomic ratios 2.0 (K_2UO_4), 1.0 ($K_2U_2O_7$), 0.5 ($K_2U_4O_{13}$) and 0.286 ($K_2U_7O_{22}$). XRD were collected for these solids during the continuous heating up to $T = 700$ °C. The authors provided a thorough discussion of their findings with regard to previous structural studies (Efremova et al., 1959; Kovba and Churbakova, 1961; Allpress et al., 1968; Anderson, 1969; Kovba, 1970, 1972; Toussaint and Avogadro, 1974). Besides the identified U(VI) compounds, the authors reported also the formation of a U(V) uranate (KUO_3) at low oxygen pressures. Jove and Cousson (1988) and Saine (1989) studied the structure of $K_2U_2O_7$(cr) by single crystal analysis with solid phases synthesized at 1200 °C and 1000 °C, respectively. Jove and co-workers reported a trigonal structure with symmetry $R\bar{3}m$, whereas Saine obtained a monoclinic form of $K_2U_2O_7$(cr) crystallising in the space group $P2_1$. Nipruk and co-workers reported the synthesis and characterization of the potassium uranates $K_2U_4O_{13}{\cdot}2.2H_2O$(cr), $K_2U_6O_{19}$(cr) (Nipruk et al., 2015) and $K_2[(UO_2)_6O_4(OH)_6]{\cdot}8H_2O$(cr) or $K_2U_6O_{19}{\cdot}11H_2O$(cr), compreignacite, Nipruk et al. (2017). Solid phases were synthesized under mildly hydrothermal conditions (100–200 °C), and pH was reported as key parameter in defining the stoichiometry K:U of the resulting compound.

The summary above highlights that most of the available studies on the system K–U(VI)–O are solid-state investigations based upon highly crystalline solids synthesized at elevated temperatures. The only available solution chemistry studies conducted at room temperature focussed on acidic pH conditions, leaving aside the alkaline to hyperalkaline pH-range relevant in repository science. Our work targets this gap, with the aim of identifying the solid phases controlling the solubility of U(VI) in alkaline KCl solutions and deriving the corresponding thermodynamic properties. Although the aqueous speciation of U(VI) in alkaline conditions is properly known (Altmaier et al., 2017; Guillaumont et al., 2003), our work aims at further extending the SIT model reported in Altmaier et al. (2017) to the interaction of anionic hydrolysis species with K^+, thus allowing reliable solubility and speciation calculations in alkaline, concentrated KCl solutions.

This paper is the second contribution to our publication series "Solubility of U(VI) in chloride solutions" and is dedicated to the stable oxides/hydroxides of U(VI) in alkaline KCl systems. It complements and further extends our previous work on the "*Solubility of U(VI) in chloride solutions. I. The stable oxides/hydroxides in NaCl systems, solubility products, hydrolysis constants and SIT coefficients*" by Altmaier et al. (2017). A third and fourth contributions on the solubility and hydrolysis of U(VI) in $MgCl_2$ and $CaCl_2$ systems, respectively, are currently under preparation.

[1] Limited experimental details on the preparation of the solid phase are provided in this publication, which refers to an unpublished work by the same author's group, A. I. Judge, D. Brown and J. Fuger.

Table 1
Main features obtained by solid phase characterization of the initial solid phase and selected samples equilibrated in KCl systems: XRD (position of the first observed diffraction peak), SEM–EDS (K:U ratio), quantitative chemical analysis (K:U ratio) and TG–DTA (number of hydration waters, x). Position of the first diffraction peak reported in the literature for some layered U(VI) structures provided for comparison.

Background electrolyte	pH_m[a]	XRD (°2Θ)	K:U ratio SEM–EDS	K:U ratio Chemical analysis	TG–DTA (number of H_2O)
2.68 m KCl "Starting material"	12.7	13.1	1.0	0.9	1.4
0.1 m KCl	7.7	12.8	n.m.	n.m.	n.m.
0.1 m KCl	9.9	13.1	1.0	0.9	1.3
0.1 m KCl	12.9	13.2	n.m.	0.9	1.7
0.51 m KCl	10.0	13.2	0.9	0.9	1.3
0.51 m KCl	12.9	13.2	n.m.	0.9	1.7
1.03 m KCl	9.8	13.1	1.0	0.9	1.3
1.03 m KCl	13.3	13.2	n.m.	1.0	1.7
3.31 m KCl	10.3	13.0	0.9	0.9	1.3
3.31 m KCl	13.3	13.2	n.m.	1.0	1.7
4.58 m KCl	10.2	13.0	1.0	*1.3*	1.3
4.58 m KCl	13.2	13.1	n.m.	1.0	1.7
average[b]			**(1.0 ± 0.1)**	**(0.9 ± 0.1)**[c]	**(1.5 ± 0.3)**
$UO_3{\cdot}2H_2O$(cr) Altmaier et al. (2017)		12.0			
$Na_2U_2O_7{\cdot}H_2O$ (cr) Altmaier et al. (2017)		14.9			
K_2UO_4(cr) JCPDS file Nr. 72–2228		13.5			
$K_2U_2O_7$(cr) JCPDS file Nr. 29–1058		13.4			
$K_2U_4O_{13}$(cr) JCPDS file Nr. 29–1059		12.6			
$K_2U_6O_{19}{\cdot}11H_2O$ (cr) JCPDS file Nr. 33–1049 Nipruk et al. (2017)		11.9			

a. ± 0.05. **b**. uncertainty calculated as 2σ. **c**. Results obtained in 4.50 m KCl at pH_m = 10.2 disregarded for calculating average and uncertainty; **n.m.** = not measured.

2. Experimental

2.1. Chemicals

Potassium chloride EMSURE® (KCl), KOH Titrisol© and HCl Titrisol© were purchased from Merck. Ethanol (99%) was provided from VWR Chemicals. All solutions were prepared with purified water (Milli–Q academic, Millipore, 18.2 MΩ cm) and purged with Ar for at least 1 h before use to remove CO_2(g) dissolved in solution. All sample preparation and handling was performed in an Ar–glove box (O_2 < 1 ppm) at T = (22 ± 2)°C.

2.2. pH measurements

The proton concentration (as pH_m, with pH_m = –log [H^+] in molal units, mol/kg_w) was measured using combination pH electrodes (ROSS Orion, with 3 M KCl as filling solution) calibrated against standard pH buffers (pH 7–12, Merck). The values of pH_m were obtained from the measured pH_{exp} values considering $pH_m = pH_{exp} + A_m$. The correction factors A_m entail both the activity coefficient of H^+ and the liquid junction potential of the electrode for the given background electrolyte concentration (Altmaier et al., 2003). The empirical correction factors A_m for KCl systems were reported previously in Baumann et al. (2017). In the systems with [OH^-] > 0.03 m, [H^+] was calculated from the known hydroxide concentration and the conditional ion product (K'_w) of water.

2.3. Solid phase preparation and characterization

A nitrate-free U(VI) stock solution was prepared by the slow precipitation of metaschoepite, $UO_3{\cdot}2H_2O$(cr), from a 0.5 M $UO_2(NO_3){\cdot}2H_2O$ solution in the pH range 4–5. The supernatant of the resulting suspension was separated after centrifugation for 10 min at 4000 g, and the solid phase was dissolved in 1 M HCl. This procedure was repeated until obtaining no nitrate signal with colorimetric test strips (< 10 ppm MQuant®). About 300 mg of $K_2U_2O_7{\cdot}xH_2O$(cr) were prepared by the slow addition (≈15 μL·min^{-1}) of a nitrate-free 0.48 M U(VI) stock solution to a 2.43 M KCl + 0.07 M KOH solution under Ar atmosphere. The resulting solid phase was aged for 2 months at T = (22 ± 2)°C and then characterized by XRD, SEM–EDS, quantitative chemical analysis and thermogravimetry – differential thermal analysis (TG–DTA). An aliquot of the solid phase (~1 mg) was washed 5–6 times with 1 mL ethanol under Ar-atmosphere to remove the matrix solution (containing KCl and KOH). After the last cleaning step, the solid was re-suspended in ethanol, deposited on a XRD sample plate, dried under Ar atmosphere for a few minutes and transferred outside the glovebox for the collection of the XRD diffractogram. XRD measurements were performed on a Bruker AXS D8 Advance X-Ray powder diffractometer (Cu anode) at measurement angle 2θ = 5–60° with incremental steps of 0.02° and a measurement time of 1.5 s per step. The diffractograms obtained were compared to the Joint Committee on Powder Diffraction Standards data base (JCPDS (2001)). After completing the XRD measurement, the solid phase was dissolved in 2% HNO_3 and taken for quantitative chemical analysis. The concentration of U and K in the resulting solution was quantified by ICP–MS (inductively coupled plasma mass spectrometry, Perkin Elmer ELAN 6100) and ICP–OES (inductively coupled plasma–optical emission spectroscopy, Perkin–Elmer 4300 DV), respectively. A second fraction of the washed solid was characterized by SEM–EDS using a Quanta 650 FEG apparatus equipped with a Noran EDS unit. The number of hydration waters in $K_2U_2O_7{\cdot}xH_2O$(cr) was quantified by TG–DTA with a Netzsch STA 449C equipment. Three samples were prepared for this purpose: (i) 29.9 mg of the initial solid phase precipitated in alkaline KCl media, (ii) 19.1 mg of the solid phase equilibrated under weakly alkaline pH conditions (9.5 ≤ pH_m ≤ 10.5) in dilute to concentrated KCl systems, and (iii) 12.1 mg of the solid phase equilibrated under hyperalkaline pH conditions (11 ≤ pH_m ≤ 14) in dilute to concentrated KCl systems. The three samples were washed 5 times with ethanol to remove the matrix solution containing KCl and KOH, left to dry for 2 days under Ar atmosphere and then transferred to a glove box exclusively dedicated to TG–DTA analysis. Measurements were performed up to T = 900 °C at a rate of 10 K min^{-1}.

2.4. Preparation of solubility samples and solubility measurements

The solubility of $K_2U_2O_7{\cdot}xH_2O$(cr) solid phase was investigated from undersaturation conditions at T = (22 ± 2) °C under Ar-atmosphere. $K_2U_2O_7{\cdot}xH_2O$(cr) was equilibrated in independent batch samples in 0.1, 0.51, 1.03, 3.31 and 4.58 m KCl solutions (0.1, 0.5, 1.0, 3.0 and 4.0 M KCl). The values of pH_m in the investigated systems were adjusted to 7.5 ≤ pH_m ≤ 14.6 by using HCl and KOH (0.001–1.0 M) of adequate ionic strength (adjusted with KCl). This resulted in a total of 34 independent batch experiments. For each sample, approximately 5 mg of $K_2U_2O_7{\cdot}xH_2O$(cr) were added to 20 mL of background solution in 50 mL screw cap centrifuge vials (Nalgene™, Thermo Scientific) after a

washing step with the corresponding background solution. Concentration of uranium and pH_m were measured at regular time intervals from 6 to 250 days. For each measurement of [U], a fraction of the supernatant (50–800 μL) of each sample was centrifuged for 2–10 min with 10 kD filters (2–3 nm cut-off Nanosep® centrifuge tubes, Pall Life Sciences) to separate colloids or suspended solid particles. After centrifugation, a known volume of the filtrate was diluted (1:100 to 1:4000, depending upon U and salt concentration) in 2% HNO_3, and concentration of uranium was quantified by ICP–MS. The accuracy of ICP–MS measurements was ± 2–5%. Detection limits (quantified as 3 times the standard deviation of repeated blank measurements) ranged between $\approx 10^{-8}$ and $\approx 10^{-10}$ M depending upon salt concentration and corresponding dilution factor. Concentration values obtained in molar units (M) were converted to molal units (m) using the conversion factors reported in the NEA–TDB (Guillaumont et al., 2003).

Thermodynamic equilibrium was assumed after repeated measurements over time showing constant [U] and pH_m. After attaining equilibrium conditions, solid phases of selected solubility samples were characterized by XRD, SEM–EDS, quantitative chemical analysis and TG–DTA as described in the previous section.

3. Results and discussion

3.1. Solid phase characterization

Table 1 summarizes the main results of the solid phase characterization obtained by XRD, SEM–EDS, quantitative chemical analysis and TG–DTA. Diffraction patterns of the initial U(VI) solid phase ("Starting material") are compared in Fig. 1a with those of $UO_3{\cdot}2H_2O$(cr), $Na_2U_2O_7H_2O$(cr) and different K–U(VI)–O/OH(s) compounds reported in the literature. These U(VI) compounds show a layered structure characterized by a strong diffraction peak at small angles (Van Egmond and Cordfunke, 1976; Saine, 1989; Nipruk et al., 2015, 2017; Altmaier et al., 2017), which can be used as fingerprint for the identification of less crystalline solid phases. The first peak in the diffractogram of the "Starting material" is found at 2Θ = 13.1°, a value remarkably different that from those reported for $UO_3{\cdot}2H_2O$(cr) (2Θ = 12.0) or $Na_2U_2O_7H_2O$(cr) (2Θ = 14.9°) (Altmaier et al., 2017), and in moderate agreement with 2Θ = 13.4° reported for $K_2U_2O_7$(cr) (JCPDS file Nr. 29–1058). Fig. 1b and c shows that the solid phases equilibrated in 0.1, 0.51, 1.03, 3.31 and 4.58 m KCl solutions at $9.5 \leq pH_m \leq 10.5$ and $12.5 \leq pH_m \leq 13.5$, respectively, retain the same XRD patterns of the original material, thus indicating that no measurable transformation of the solid phase took place during the solubility experiments. The only exception is found for the solid phase recovered from the solubility sample in 0.1 m KCl at $pH_m = 7.7$, which shows sharper patterns and a shift of the first peak in the diffractogram to 2Θ ≈ 12.8° (see Fig. 1b). This observation suggests that a solid phase transformation occurred at this pH_m and salt concentration. According to the trend in 2Θ values of potassium uranate compounds ($K_2U_2O_7$(cr), $K_2U_4O_{13}$(cr) and $K_2U_6O_{19}{\cdot}11H_2O$(cr), see Table 1), the shift of the first peak to lower 2Θ values suggests a decrease in the K:U stoichiometry of the solid phase controlling the solubility of U(VI) in this sample. Similar observations were reported in solubility experiments with U(VI) and Np(VI) in NaCl systems (Diaz-Arocas and Grambow, 1998; Gaona et al., 2013; Endrizzi et al., 2018).

The ratio K:U in the solid phase of selected solubility samples was quantified as (1.0 ± 0.1) and (0.9 ± 0.1) by SEM–EDS and quantitative chemical analysis, respectively. These values are also in excellent agreement with the K:U ratio quantified for the "Starting material". The K:U ratio determined for the solid phase recovered from the solubility sample at $pH_m = 10.2$ in 4.58 m KCl is abnormally high (K:U = 1.3), and likely reflects the insufficient washing step in this highly concentrated KCl system. Together with XRD data, results obtained by

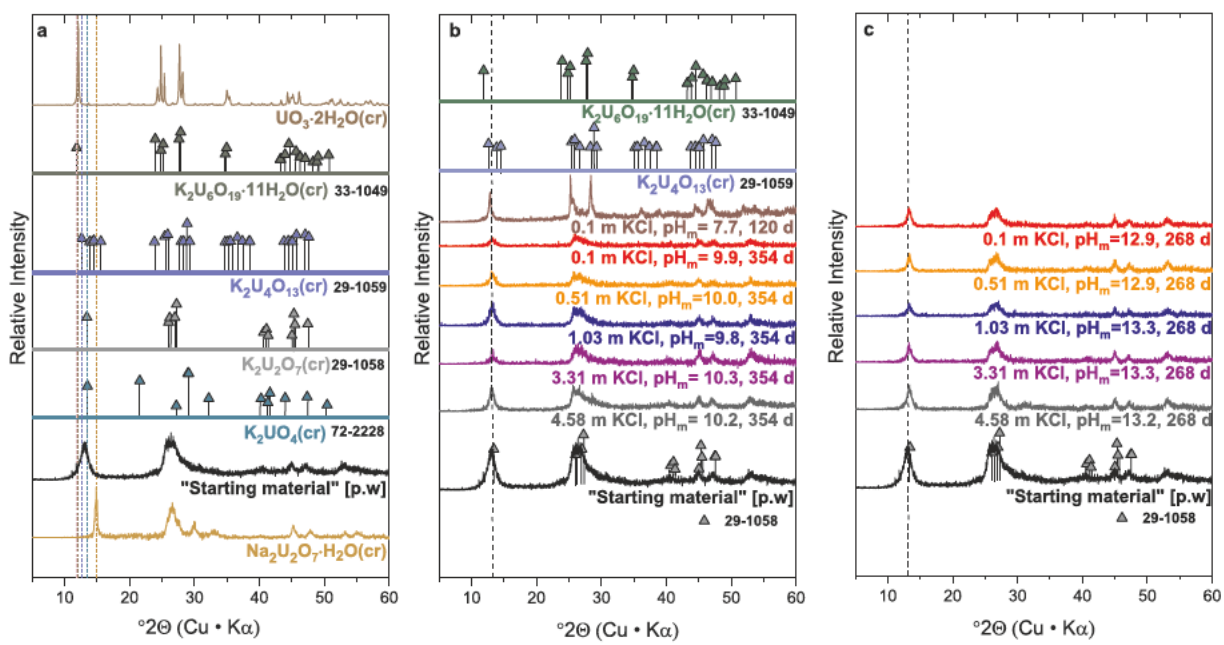

Fig. 1. XRD patterns of solid phases recovered from selected solubility experiments in dilute to concentrated KCl solutions: a. Comparison between "Starting material" synthesized in the present work, XRD patterns reported by Altmaier et al. (2017) for $Na_2U_2O_7H_2O$(cr) and $UO_3{\cdot}2H_2O$(cr), and reference data (peak positions and relative intensities) reported in the JCPDS database for $K_2U_6O_{19}{\cdot}11H_2O$(cr) (JCPDS file Nr. 33–1049), $K_2U_4O_{13}$(cr) (JCPDS file Nr. 29–1059), $K_2U_2O_7$(cr) (JCPDS file Nr. 29–1058) and K_2UO_4(cr) (JPDS file Nr. 72–2228); b. Comparison between "Starting material" synthesized in the present work and solid phases recovered from solubility experiments at pH_m = 9.5–10.5 after t = 354 days. Peak positions and relative intensities of $K_2U_2O_7$(cr) (JCPDS file Nr. 29–1058), $K_2U_4O_{13}$(cr) (JCPDS file Nr. 29–1059) and $K_2U_6O_{19}{\cdot}11H_2O$(cr) (JCPDS file Nr. 33–1049) provided for comparison; c. Comparison between "Starting material" synthesized in the present work and solid phases recovered from solubility experiments at pH_m = 12.5–13.5 after t = 268 days. Peak positions and relative intensities of $K_2U_2O_7$(cr) (JCPDS file Nr. 29–1058) provided for comparison.

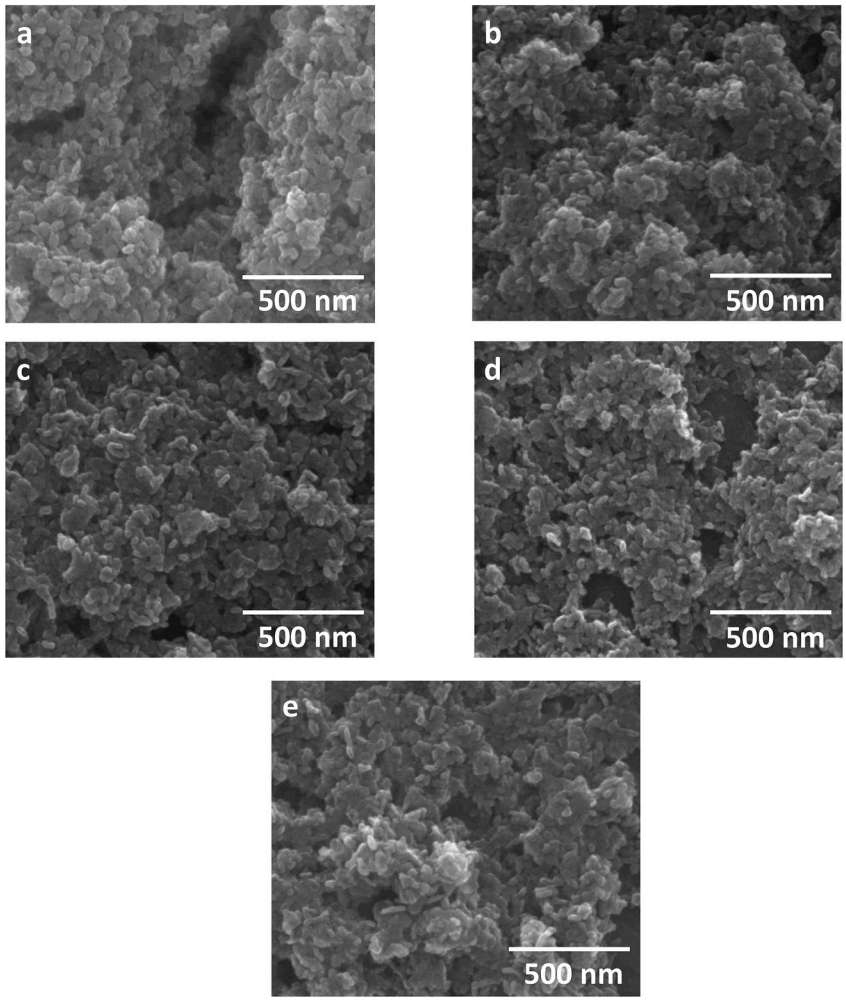

Fig. 2. SEM images of $K_2U_2O_7{\cdot}1.5H_2O$(cr) solid phase equilibrated at $pH_m \sim 10$ in a. 0.1 m KCl, b. 0.51 m KCl c. 1.03 m KCl, d. 3.31 m KCl and e. 4.58 m KCl.

SEM–EDS and quantitative chemical analysis support that the solid phase $K_2U_2O_7{\cdot}xH_2O$(cr) controls the solubility of U(VI) in all investigated KCl–KOH systems (with the only exception reported above). TG–DTA analyses performed for the dried solid phases collected from the "Starting material" and selected solubility samples lead to similar results in all cases (x = 1.3–1.7 in $K_2U_2O_7{\cdot}xH_2O$(cr)). The unweighted average (1.5 ± 0.3) is considered as the number of hydration waters of the solid phase under investigation, $K_2U_2O_7{\cdot}1.5H_2O$(cr).

Fig. 2 shows the SEM images of solid phases recovered from selected solubility experiments in 0.1, 0.51, 1.03, 3.31 and 4.58 m KCl, all of them at $pH_m \approx 10$. All images show solid phases with similar shape (platelet–like structures) and size, again supporting that the same solid phase controls the solubility of U(VI) in all investigated systems.

3.2. Solubility measurements

Fig. 3 shows solubility data determined for $K_2U_2O_7{\cdot}1.5H_2O$(cr) in 0.1, 0.51, 1.03, 3.31 and 4.58 m KCl systems at $7.5 \leq pH_m \leq 14.6$. Under hyperalkaline conditions ($pH_m \geq 11$), the solubility increases with increasing pH_m following a well-defined slope of +1 (log [U] *vs.* pH_m). This observation indicates the release of one H^+ in the equilibrium reaction controlling the solubility of U(VI) in this pH_m-region. These results are consistent with the solubility reaction 0.5 $K_2U_2O_7{\cdot}1.5H_2O$(cr) + 1.75 H_2O(l) ⇔ $UO_2(OH)_4^{2-}$ + H^+ + K^+, which is further supported by solid phase characterization described in Section 3.1 and the known aqueous speciation of U(VI) under hyperalkaline conditions (Grenthe et al., 1992; Altmaier et al., 2017; Guillaumont et al., 2003). In this pH_m-region, a decrease in solubility of ≈1.5 orders of magnitude is observed when increasing the concentration of KCl from 0.1 to 4.50 m. A similar trend was reported by Altmaier et al. (2017) for the solubility of $Na_2U_2O_7{\cdot}H_2O$(cr) at analogous pH_m and background electrolyte concentration, thus highlighting the similar ion interactions driven by Na^+ and K^+ cations.

A pH_m-independent solubility behaviour is observed at $pH_m < \sim 11$ regardless of ionic strength. Slope analysis and solid phase characterization indicate that the equilibrium reaction 0.5 $K_2U_2O_7{\cdot}1.5H_2O$(cr) + 0.75 H_2O(l) ⇔ $UO_2(OH)_3^-$ + K^+ controls the solubility of U(VI), in excellent agreement with analogous solubility experiments with $Na_2U_2O_7{\cdot}H_2O$(cr) and the known aqueous speciation of U(VI) (Grenthe et al., 1992; Altmaier et al., 2017; Guillaumont et al., 2003). Solubility data collected in this pH_m-region show a large scattering of up to one order of magnitude due to very low concentration of uranium, close to the detection limit of the measurement technique. Similar observations have been reported for the solubility of U(VI) in alkaline, dilute to concentrated NaCl systems (Altmaier et al., 2017; Endrizzi et al., 2018).

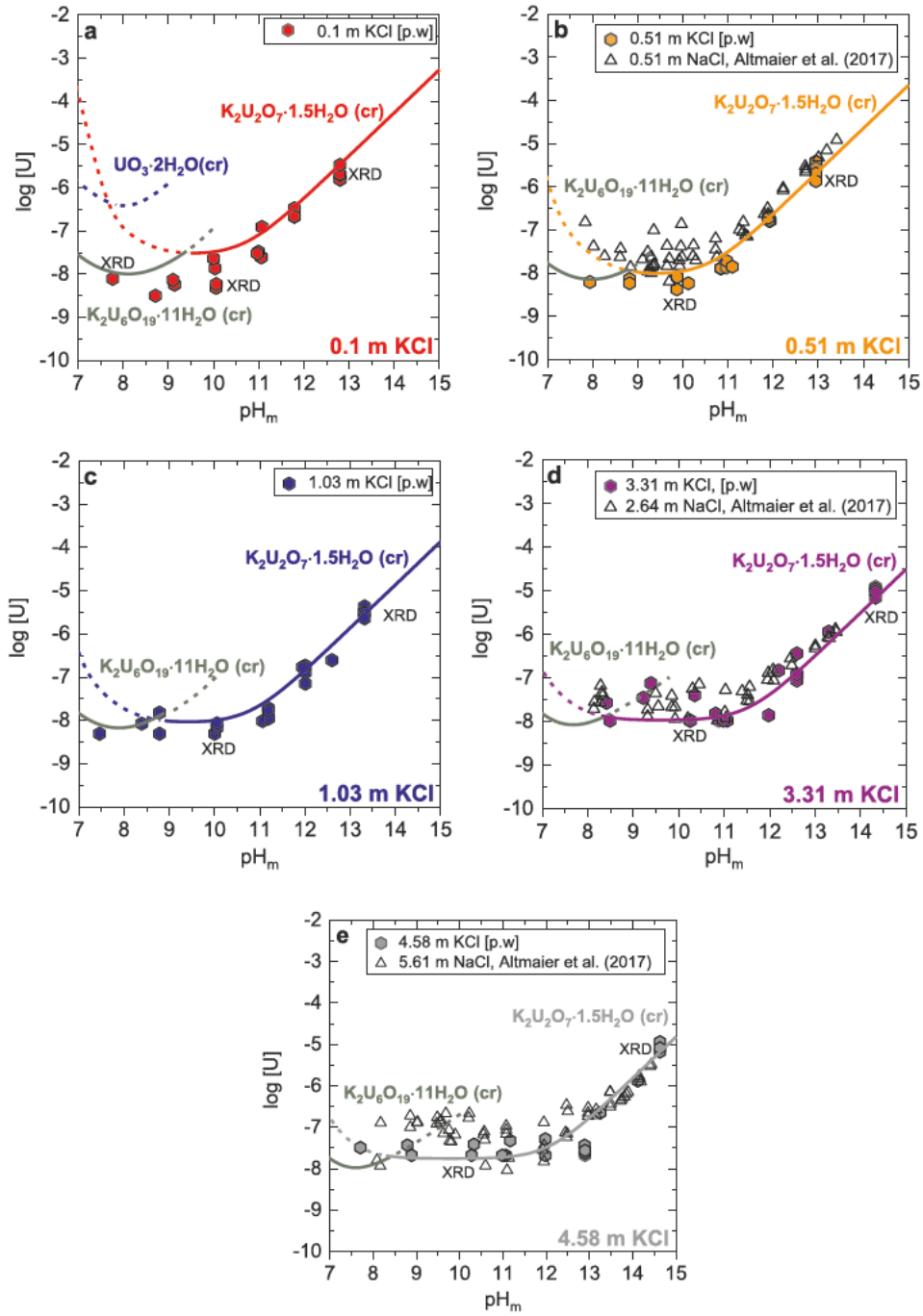

Fig. 3. Solubility of $K_2U_2O_7 \cdot 1.5H_2O$(cr) in alkaline KCl solutions: a. 0.1 m; b. 0.51 m, c. 1.03 m, d. 3.31 m and e. 4.58 m. Black triangles correspond to the solubility of $Na_2U_2O_7 \cdot H_2O$(cr) reported by Altmaier et al. (2017) in 0.5, 2.64 and 5.61 m NaCl systems. Lines are solubilities of $UO_3 \cdot 2H_2O$(cr), $K_2U_6O_{19} \cdot 11H_2O$(cr) and $K_2U_2O_7 \cdot 1.5H_2O$(cr) calculated with thermodynamic and SIT activity models summarized in Tables 2 and 3.

4. Chemical, thermodynamic and SIT activity models

Chemical models derived above based upon slope analysis and solid phase characterization are used in this section to fit solubility data in 0.1–4.58 m KCl, and accordingly derive thermodynamic and activity models for the investigated system. Conditional constants log $^*K^\circ_{s,(1,4)}$ derived from solubility data at pH_m above ≈ 11 are used to obtain log $^*K^\circ_{s,(1,4)}$ and $\varepsilon(UO_2(OH)_4^{2-}, K^+)$ following the SIT approach (Ciavatta, 1980). The combination of log $^*K^\circ_{s,(1,4)}$ with the hydrolysis constant log $^*\beta^\circ_{(1,4)}$ reported in Altmaier et al. (2017) allows the determination of log $^*K^\circ_{s,0}\{0.5\ K_2U_2O_7 \cdot 1.5H_2O(cr)\}$. Experimental data obtained in the present work at $pH_m \leq 11$ are not used to derive new thermodynamic data, but are compared to the solubility calculated using log $^*K^\circ_{s,0}\{0.5\ K_2U_2O_7 \cdot 1.5H_2O(cr)\}$ determined in this work and U(VI) hydrolysis constants reported in Altmaier et al. (2017). Solubility data reported in Sandino and Grambow (1994) and Gorman-Lewis et al. (2008b) for $K_2U_6O_{19} \cdot 11H_2O$(cr) (compreignacite) are re-evaluated in Section 4.2 consistently with thermodynamic and activity models considered in this work for U(VI) hydrolysis species (see Section 4.3). The updated thermodynamic model for the system UO_2^{2+}–H^+–K^+–Na^+–Cl^-–OH^-–H_2O (l) is used in Section 4.4 to evaluate the role of hydrated Na- and K-uranates in controlling the solubility of U(VI) in alkaline, cementitious environments.

4.1. Thermodynamic data derived from U(VI) solubility experiments in alkaline KCl systems

Solubility data of U(VI) in dilute to concentrated KCl solutions at $pH_m \geq 11$ are adequately explained by the equilibrium reaction (1):

$$0.5\ K_2U_2O_7{\cdot}1.5H_2O(cr) + 1.75\ H_2O(l) \Leftrightarrow UO_2(OH)_4^{2-} + H^+ + K^+ \quad (1)$$

with

$$\log {}^*K'_{s,(1,4)} = \log [UO_2(OH)_4^{2-}] + \log[H^+] + \log[K^+] \quad (2)$$

$$\log {}^*K^o_{s,(1,4)} = \log {}^*K'_{s,(1,4)} + \log \gamma_{UO_2(OH)_4^{2-}} + \log \gamma_{H^+} + \log \gamma_{K^+} - 1.75 \log a_w \quad (3)$$

Conditional solubility constants $\log {}^*K'_{s,(1,4)}$ are obtained by independently fitting solubility datasets in 0.1–4.58 m KCl following equation (2). Equation (3) is used to extrapolate the values of $\log {}^*K'_{s,(1,4)}$ to $I = 0$, thus resulting in $\log {}^*K^\circ_{s,(1,4)}$ and $-\Delta\varepsilon$. The combination of the latter value with $\varepsilon(H^+, Cl^-)$ and $\varepsilon(K^+, Cl^-)$ as reported in the NEA–TDB allows also calculating the SIT interaction coefficient $\varepsilon(UO_2(OH)_4^{2-}, K^+)$. Fig. 4 shows the linear regression $\log {}^*K'_{s,(1,4)} - 6\ D - 1.75 \log a_w$ *vs.* [KCl] (SIT-plot). For comparative purposes, the figure shows also the SIT-plot for the analogous equilibrium reaction in NaCl systems $\log {}^*K'_{s,(1,4)} - 6\ D - 2\log a_w$ *vs* [NaCl], with $Na_2U_2O_7{\cdot}H_2O(cr)$ as solubility-controlling phase) reported in Altmaier et al. (2017).

The SIT-plot in Fig. 4 results in $\log {}^*K^\circ_{s,(1,4)}\{0.5\ K_2U_2O_7{\cdot}1.5H_2O(cr)\} = -(19.90 \pm 0.06)$ as the intercept of the linear regression. This value is of the same order but slightly lower than $\log {}^*K^\circ_{s,(1,4)}\{0.5\ Na_2U_2O_7{\cdot}H_2O(cr)\} = -(19.7 \pm 0.1)$ reported by Altmaier et al. (2017) based upon analogous solubility experiments in NaCl solutions. The slope of the linear regression ($-\Delta\varepsilon = -[\varepsilon(UO_2(OH)_4^{2-}, K^+) + \varepsilon(H^+, Cl^-) + \varepsilon(K^+, Cl^-)] = -(0.15 \pm 0.04)$ kg·mol^{-1}) is combined with $\varepsilon(K^+, Cl^-) = (0.0 \pm 0.01)$ kg·mol^{-1} and $\varepsilon(H^+, Cl^-) = (0.12 \pm 0.01)$ kg·mol^{-1} reported in NEA–TDB (Grenthe et al., 1992; Guillaumont et al., 2003) to obtain $\varepsilon(UO_2(OH)_4^{2-}, K^+) = (0.03 \pm 0.04)$ kg·mol^{-1}. This value is in excellent agreement with $\varepsilon(UO_2(OH)_4^{2-}, Na^+) = (0.01 \pm 0.04)$ kg·mol^{-1} reported in Altmaier et al. (2017), as expected from the similar slope in the SIT-plot of KCl/NaCl systems in Fig. 4.

The solubility constant $\log {}^*K^\circ_{s,0}\{0.5\ K_2U_2O_7{\cdot}1.5H_2O(cr)\}$ is calculated combining $\log {}^*K^\circ_{s,(1,4)}\{0.5\ K_2U_2O_7{\cdot}1.5H_2O(cr)\}$ determined in the present work and $\log {}^*\beta^\circ_{(1,4)} = -(31.9 \pm 0.2)$ reported by Altmaier et al. (2017), resulting in:

$$0.5\ K_2U_2O_7{\cdot}1.5H_2O(cr) + 3\ H^+ \Leftrightarrow UO_2^{2+} + K^+ + 2.25\ H_2O(l) \quad (4)$$

$\log {}^*K^\circ_{s,0}\{0.5\ K_2U_2O_7{\cdot}1.5H_2O(cr)\} = \log {}^*K^\circ_{s,(1,4)} - \log {}^*\beta^\circ_{(1,4)} = (12.0 \pm 0.2)$ (p.w.)

This value is slightly lower than the solubility determined by Altmaier et al. (2017) for $Na_2U_2O_7{\cdot}H_2O(cr)$, $\log {}^*K^\circ_{s,0}\{0.5Na_2U_2O_7{\cdot}H_2O(cr)\} = (12.2 \pm 0.2)$. The relevance of both solid phases in different cementitious systems is discussed in Section 4.4.

No efforts have been done to attempt the fit of the solubility data of $K_2U_2O_7{\cdot}1.5H_2O(cr)$ below $pH_m \approx 11$. Instead, the accurate value of $\log {}^*K^\circ_{s,0}\{0.5\ K_2U_2O_7{\cdot}1.5H_2O(cr)\}$ derived from the pH_m-region where $UO_2(OH)_4^{2-}$ predominates has been favoured. Hydrolysis constants reported in Altmaier et al. (2017) for $UO_2(OH)_3^-$ (13) and $(UO_2)_3(OH)_7^-$ (37) species (both of them forming in the pH_m-region under discussion) have been preferred for the overall thermodynamic model of U(VI) (see Section 4.3 and Tables 2 and 3). Considering the excellent agreement observed between $\varepsilon(UO_2(OH)_4^{2-}, K^+)$ and $\varepsilon(UO_2(OH)_4^{2-}, Na^+)$, ion interaction coefficient for (1,3) and (3,7) species with K^+ are taken as $\varepsilon(UO_2(OH)_3^-, K^+) = \varepsilon(UO_2(OH)_3^-, Na^+) = -(0.24 \pm 0.09)$ kg·mol^{-1} and $\varepsilon((UO_2)_3(OH)_7^-, K^+) = \varepsilon((UO_2)_3(OH)_7^-), Na^+) = -(0.24 \pm 0.09)$ kg mol^{-1}.

4.2. Re-evaluation of log *K°s,0{1/6 K2U6O19·11H2O(cr)} (compreignacite) reported in the literature in 1 m KCl

The solubility of $K_2U_6O_{19}{\cdot}11H_2O(cr)$ was previously investigated by Sandino and Grambow (1994) and Gorman-Lewis et al. (2008b) (see detailed discussion in the introduction). Although both studies targeted acidic conditions ($3.5 \leq pH \leq 5$), the actual stability field of compreignacite may further extend to near-neutral and weakly alkaline KCl systems. Thus this solid phase justifies a detailed re-evaluation in the context of this study. In order to ensure internal consistency when using $\log {}^*K^\circ_{s,0}\{1/6\ K_2U_6O_{19}{\cdot}11H_2O(cr)\}$, the original solubility data are re-evaluated in this section using the thermodynamic and activity models summarized in Tables 2 and 3 for U(VI) hydrolysis species. Accordingly, the only unknown parameter is $\log {}^*K^\circ_{s,0}\{1/6\ K_2U_6O_{19}{\cdot}11H_2O(cr)\}$ corresponding to the equilibrium reaction (5), which is determined by minimizing the function $\Sigma((\log [U]_{exp} - \log [U]_{calc})^2)^{1/2})$. Only the data reported by Sandino and Grambow (1994) are considered for the determination of $\log {}^*K^\circ_{s,0}\{1/6\ K_2U_6O_{19}{\cdot}11H_2O(cr)\}$. Solubility data reported by Gorman–Lewis et al. (2008b) are disregarded in this exercise because of the large variation in the ionic strength between different solubility samples (from ≈0.006 to ≈ 0.3 M) and the short equilibration times considered by the authors (9–27 days). The values of pH originally reported by Sandino and Grambow have been converted in this work to pH_m by SIT using $\varepsilon(H^+, Cl^-) = (0.12 \pm 0.01)$ kg·mol^{-1} as reported in the NEA–TDB (Guillaumont et al., 2003).

$$1/6\ K_2U_6O_{19}{\cdot}11H_2O(cr) + 7/3\ H^+ \Leftrightarrow UO_2^{2+} + 1/3\ K^+ + 3\ H_2O(l) \quad (5)$$

with

$$\log {}^*K'_{s,0} = \log [UO_2^{2+}] - \frac{7}{3} \log[H^+] + \frac{1}{3} \log[K^+] \quad (6)$$

$$\log {}^*K^o_{s,0} = \log {}^*K'_{s,0} + \log \gamma_{UO_2^{2+}} - \frac{7}{3} \log \gamma_{H^+} + \frac{1}{3} \log \gamma_{K^+} + 3 \log a_w \quad (7)$$

The fit of $\log {}^*K^\circ_{s,0}\{1/6\ K_2U_6O_{19}{\cdot}11H_2O(cr)\}$ in the two independent datasets reported by Sandino and Grambow (1994) results in:

$\log {}^*K^\circ_{s,0}(\text{run K1}) = (6.1 \pm 0.1)$

$\log {}^*K^\circ_{s,0}(\text{run K2}) = (6.5 \pm 0.1)$

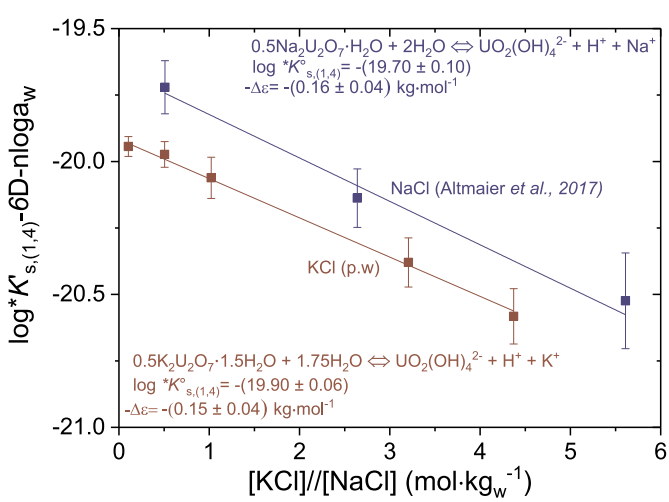

Fig. 4. SIT-plot for the solubility reactions $0.5\ M_2U_2O_7{\cdot}xH_2O(cr) + (2.5–0.5x)\ H_2O(l) \Leftrightarrow UO_2(OH)_4^{2-} + H^+ + M^+$ (with M = K or Na) using experimental $\log {}^*K'_{s,(1,4)}$ values determined in dilute to concentrated KCl (present work) and NaCl (Altmaier et al., 2017) solutions. Term "n" in y-axis = 1.75 and 2 for KCl and NaCl systems, respectively.

As discussed by Sandino and Grambow, differences between log $^*K^\circ_{s,0}$(run K1) and log $^*K^\circ_{s,0}$(run K2) likely reflect slight differences in the crystallinity of both solid phases. The unweighted average log $^*K^\circ_{s,0}\{1/6\ K_2U_6O_{19}{\cdot}11H_2O(cr)\}$ = (6.3 ± 0.1) is used to calculate the solubility curve in Fig. 5, and is included in the list of selected values in Table 2. This value agrees within the uncertainties with the NEA–TDB selection (log $^*K^\circ_{s,0}$ = (6.18 ± 0.09)), but is now internally consistent with the hydrolysis scheme, equilibrium constants and SIT coefficients considered in the present work.

4.3. Summary of chemical, thermodynamic and activity models for the system UO_2^{2+}–H^+–K^+–Na^+–Cl^-–OH^-–H_2O (l)

Tables 2 and 3 summarize the chemical, thermodynamic and SIT activity models for the system UO_2^{2+}–H^+–K^+–Na^+–Cl^-–OH^-–H_2O(l) as discussed in Sections 4.1 and 4.2 of this new study or reported in Guillaumont et al. (2003) and Altmaier et al. (2017). These models are used to calculate the solubility of $K_2U_2O_7{\cdot}1.5H_2O$(cr) and $K_2U_6O_{19}{\cdot}11H_2O$(cr) in 0.1–4.58 m KCl solutions at $7 \le pH_m \le 14.5$, and compared in Fig. 3 to experimental solubility data determined in the present study.

Experimental solubility data are generally in good agreement with the solubility calculated for $K_2U_2O_7{\cdot}1.5H_2O$(cr), although relevant deviations occur at low KCl concentration (≤0.51 m) and pH_m (≤9.5) values. Such discrepancies can be rationalized by the presence of other solid phases controlling the solubility of U(VI) under these boundary conditions, as further supported by XRD (see Section 3.1, sample in 0.1 m KCl at pH_m = 7.7). The calculated solubility of $K_2U_6O_{19}{\cdot}11H_2O$ (cr) provides indeed a good explanation for the observed deviations, although the XRD patterns obtained for the solid equilibrated in 0.1 m KCl at pH_m = 7.7 do not match those reported for compreignacite. We hypothesize that other sub-stoichiometric potassium uranate compounds are responsible for the control of U(VI) solubility in these conditions.

The set of equilibrium constants and SIT coefficients summarized in Tables 2 and 3 provides a satisfactory and consistent explanation of U (VI) spectroscopic, potentiometric and solubility observations reported in dilute to concentrated KCl (present work and Sandino and Grambow, 1994), NaCl solutions (Altmaier et al., 2017 and references therein). Although the fit of each independent dataset may result in improved statistical parameters, we favour a data selection able to explain all available experimental observations. This results in a comprehensive and internally consistent model for the investigated system.

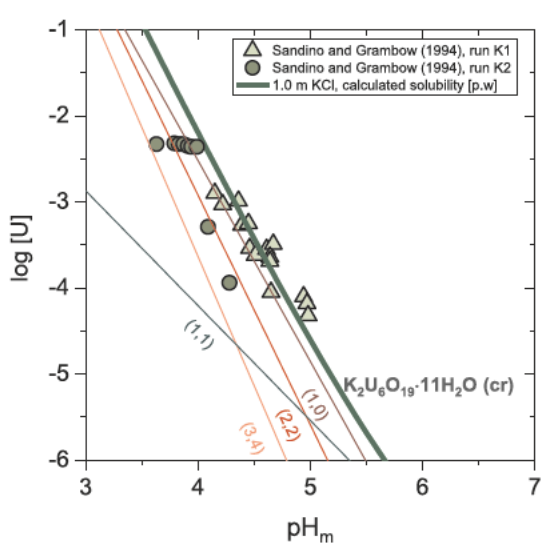

Fig. 5. Solubility of U(VI) in 1 m KCl solutions at $3 \le pH_m \le 6$ as reported by Sandino and Grambow (1994) (runs K1 and K2 in the original publication, see discussion in text). Solid lines correspond to the solubility of $K_2U_6O_{19}{\cdot}11H_2O$ (cr) (thick line) and underlying aqueous speciation (thin lines) calculated with the thermodynamic and SIT activity models summarized in Tables 2 and 3.

Table 2
Solubility and hydrolysis constants at I = 0 selected in the present work for the system UO_2^{2+}–H^+–K^+–Na^+–Cl^-–OH^-–H_2O(l).

Solid phases		log $^*K^\circ_{s,0}$	References
0.5 $K_2U_2O_7{\cdot}1.5H_2O$(cr)		(12.0 ± 0.2)	(p.w.)
1/6 $K_2U_6O_{19}{\cdot}11H_2O$(cr)		(6.3 ± 0.1)	(p.w.), [a]
0.5 $Na_2U_2O_7{\cdot}H_2O$(cr)		(12.2 ± 0.2)	(Altmaier et al., 2017)
Hydrolysis species	**(*xy*)**	**log $^*\beta^\circ_{(x,y)}$**	
UO_2OH^+	(11)	−(5.25 ± 0.24)	(Guillaumont et al., 2003)
$UO_2(OH)_2$(aq)	(12)	−(12.15 ± 0.17)	(Guillaumont et al., 2003)
$UO_2(OH)_3^-$	(13)	−(20.7 ± 0.40)	(Altmaier et al., 2017)
$UO_2(OH)_4^{2-}$	(14)	−(31.9 ± 0.2)	(Altmaier et al., 2017)
$(UO_2)_2(OH)_2^{2+}$	(22)	−(5.62 ± 0.04)	(Guillaumont et al., 2003)
$(UO_2)_3(OH)_4^{2+}$	(34)	−(11.9 ± 0.3)	(Guillaumont et al., 2003)
$(UO_2)_3(OH)_5^+$	(35)	−(15.55 ± 0.12)	(Guillaumont et al., 2003)
$(UO_2)_3(OH)_7^-$	(37)	−(32.20 ± 0.80)	(Guillaumont et al., 2003)
$(UO_2)_4(OH)_7^+$	(47)	−(21.9 ± 1.0)	(Guillaumont et al., 2003)

[a] Re-evaluated in this work from experimental data reported in Sandino and Grambow (1994).

Table 3
SIT ion interaction coefficients for UO_2^{2+} and U(VI) hydrolysis species derived in the present work and reported in the literature for NaCl and KCl systems.

U(VI) species	SIT coefficients		References
I	*J*	ε(*i*,*j*)	
UO_2^{2+}	Cl^-	(0.21 ± 0.02)	(Ciavatta, 1980)
UO_2OH^+	Cl^-	(0.10 ± 0.10)	(Altmaier et al., 2017)
$(UO_2)_2(OH)_2^{2+}$	Cl^-	(0.30 ± 0.06)	(Altmaier et al., 2017)
$(UO_2)_3(OH)_4^{2+}$	Cl^-	−(0.07 ± 0.17)	(Altmaier et al., 2017)
$(UO_2)_3(OH)_5^+$	Cl^-	(0.24 ± 0.15)	(Altmaier et al., 2017)
$(UO_2)_4(OH)_7^+$	Cl^-	(0.17 ± 0.18)	(Altmaier et al., 2017)
$UO_2(OH)_3^-$	Na^+	−(0.24 ± 0.09)	(Altmaier et al., 2017)
	K^+	−(0.24 ± 0.09)	(p.w.), [a]
$UO_2(OH)_4^{2-}$	Na^+	(0.01 ± 0.04)	(Altmaier et al., 2017)
	K^+	(0.03 ± 0.04)	(p.w.)
$(UO_2)_3(OH)_7^-$	Na^+	−(0.24 ± 0.09)	(Altmaier et al., 2017)
	K^+	−(0.24 ± 0.09)	(p.w.), [a]
$UO_2(OH)_2$(aq)	K^+, Na^+, Cl^-	0	[b]

[a] Set equal to the ion interaction coefficient of the same species with Na^+.
[b] By definition in SIT.

4.4. Na–U(VI)–OH and K–U(VI)–OH ternary solid phases in cementitious systems

Sodium and potassium are the most abundant cations in the degradation phase I of cement (Berner, 1992; Taylor, 1997; Wieland and Van Loon, 2003; Ochs et al., 2016). In salt-based repositories, the contact of concentrated NaCl brines with cement expectedly results in hyperalkaline mixed salt-systems with high concentrations of both NaCl and KCl (Bube et al., 2013). Under these conditions, the solid phases $K_2U_2O_7{\cdot}1.5H_2O$(cr) and $Na_2U_2O_7{\cdot}H_2O$(cr) may compete for controlling the solubility of U(VI) (Yamazaki et al., 1992). In our contribution to this special issue (Cevirim-Papaioannou et al., 2018), we have demonstrated that $Na_2U_2O_7{\cdot}H_2O$(cr) plays an important role in controlling the reduction of U(VI) to U(IV) in hyperalkaline NaCl systems. In this context, this section aims at evaluating the role of $K_2U_2O_7{\cdot}1.5H_2O$(cr) and $Na_2U_2O_7{\cdot}H_2O$(cr) in cementitious environments of relevance in the context of nuclear waste disposal using two "examples" at low and high ionic strength conditions.

Fig. 6 shows the solubility of both solid phases, which has been calculated for $9 \le pH_m \le 13.5$ using the thermodynamic and activity

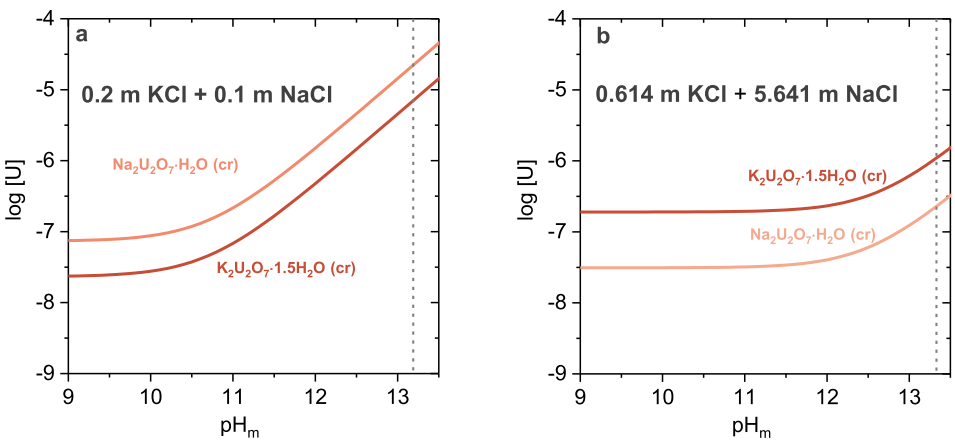

Fig. 6. Solubility of $K_2U_2O_7{\cdot}1.5H_2O$(cr) and $Na_2U_2O_7{\cdot}H_2O$(cr) at $9 \leq pH_m \leq 13.5$ in a. 0.2 m KCl +0.1 m NaCl solutions; b. 0.614 m KCl +5.641 m NaCl solutions. Calculations performed using thermodynamic and activity models summarized in Tables 2 and 3. Vertical dashed line corresponding to the pH_m in the original composition.

models summarized in Tables 2 and 3 for the systems:

i 0.1 m Na^+ + 0.2 m K^+, (Figure a): this system is representative of the degradation phase I of cement in dilute porewater systems. The concentration of sodium and potassium are controlled by the dissolution of Na_2O and K_2O, which further buffer the pH at ≈ 13.3 (or $pH_m \approx 13.2$).

ii 5.641 m Na^+ + 0.614 m K^+, (Figure b): this mixed composition was calculated in Bube et al. (2013) for cement L/ILW simulates exposed to concentrated NaCl brine solutions.[2]

Fig. 6a shows that for the dilute system (0.2 m KCl + 0.1 m NaCl), $K_2U_2O_7{\cdot}1.5H_2O$(cr) is expected to control the solubility of U(VI) at $9 \leq pH_m \leq 13.5$. This includes the conditions characteristic for the degradation Phase I of cement. On the contrary, the solubility of U(VI) in 5.641 m NaCl + 0.614 m KCl (Fig. 6b) is controlled by $Na_2U_2O_7{\cdot}H_2O$ (cr) due to the large excess of Na^+ with respect to K^+. Consequently, both compounds appear as relevant U(VI) solid phases in the context of cementitious systems depending on specific geochemical conditions, and none of the two phases can be *a priori* be ruled out.

Two important aspects require further discussion with regard to establishing a more comprehensive view of the U(VI) solubility control in cementitious environments:

- $K_2U_2O_7{\cdot}1.5H_2O$(cr) and $Na_2U_2O_7{\cdot}H_2O$(cr) solid phases share the same layered structure with alkaline ions placed in the interlayer. It may thus be possible that mixed phases of the $Na_xK_{2-x}O_7{\cdot}yH_2O$(cr) type exist, and that these are controlling the solubility of U(VI) in alkaline mixed systems. Our discussion above may in this respect therefore include a strong simplification.
- Considering the different cement degradation stages, potassium and sodium are only relevant elements in the degradation phase I of cement. Once K_2O and Na_2O are washed out, the composition of the porewater in cementitious systems is controlled by the dissolution of portlandite ($Ca(OH)_2$, degradation phase II with pH ≈ 12.5 and $[Ca]_{aq} \approx 20$ mM) and C-S-H phases (calcium-silicate-hydrates, degradation phase III with $10 \leq pH \leq 12.5$ and $1 \leq [Ca]_{aq}$ (mM) ≤ 20). Phases II and III are clearly dominated by calcium in solution and therefore Ca needs to be considered when addressing U (VI) solubility phenomena. Ca–U(VI)–OH solid phases (e.g. $CaU_2O_7{\cdot}3H_2O$(cr), Altmaier et al., 2005) can be expected to control the solubility of U(VI) under these conditions. A comprehensive study on the Ca-U(VI) system combining solubility studies and spectroscopy is currently on-going at KIT–INE and will provide an accurate thermodynamic description of this system, keeping consistency with the model established in the present study.

[2] As discussed in Baumann et al. (2017), concentrations reported in Bube et al. (2013) were decreased by 10% to avoid precipitation of saturated salts.

5. Summary and conclusions

The solubility of U(VI) was investigated from undersaturation conditions in alkaline, dilute to concentrated KCl solutions. Solid phase characterization by XRD, quantitative chemical analysis, SEM–EDS and TG–DTA confirm that $K_2U_2O_7{\cdot}1.5H_2O$(cr) controls the solubility of U (VI) above $pH_m \approx 9.5$ regardless of KCl concentration. Combining solubility data obtained in the present work with the U(VI) hydrolysis scheme reported in Altmaier et al. (2017), we determine log $^*K^\circ_{s,0}\{0.5\ K_2U_2O_7{\cdot}1.5H_2O(cr)\} = (12.0 \pm 0.2)$. The re-evaluation of available experimental data in acidic KCl solutions consistently with our hydrolysis scheme gives further insight on the solubility of compreignacite, resulting in log $^*K^\circ_{s,0}\{1/6\ K_2U_6O_{19}{\cdot}11H_2O(cr)\} = (6.3 \pm 0.1)$. The combination of these data with our previous study in NaCl systems (Altmaier et al., 2017) provides an accurate thermodynamic description of the system UO_2^{2+}–H^+–K^+–Na^+–Cl^-–OH^-–H_2O(l). Scoping calculations performed with these thermodynamic and activity models indicate that $K_2U_2O_7{\cdot}1.5H_2O$(cr) may control the solubility of U(VI) in hyperalkaline systems as those representative of the degradation phase I of cement. In weakly alkaline KCl solutions, the formation of non-stoichiometry potassium uranates with K:U < 1 must be taken into account. This work allows more accurate U(VI) source term estimations under geochemical boundary conditions relevant for nuclear waste disposal.

Acknowledgements

The authors would like to thank Melanie Böttle, Frank Geyer, Cornelia Walschburger, Eva Soballa and Nicolas Finck (all KIT–INE) for their technical support. This study was funded by the German Ministry of Economic Affairs and Energy (BMWi) within the framework of the EDUKEM project under the contract number 02E11334.

References

Allpress, J.G., Anderson, J.S., Hambly, A.N., 1968. Reaction of uranium oxides with alkali halides. J. Inorg. Nucl. Chem. 30, 1195.
Altmaier, M., Metz, V., Neck, V., Müller, R., Fanghänel, T., 2003. Solid-liquid equilibria of $Mg(OH)_2$(cr) and $Mg_2(OH)_2Cl.4H_2O$(cr) in the system Mg-Na-H-OH-O-Cl-H_2O at 25 °C. Geochem. Cosmochim. Acta 67, 3595–3601.
Altmaier, M., Neck, V., Fanghänel, T., 2005. Solubility of Uranium in Dilute to Concentrated NaCl, $MgCl_2$, and $CaCl_2$ Solutions, Migration Conference. Avignon, France.
Altmaier, M., Yalcintas, E., Gaona, X., Neck, V., Müller, R., Schlieker, M., Fanghänel, T., 2017. Solubility of U(VI) in chloride solutions. I. The stable oxides/hydroxides in NaCl systems, solubility products, hydrolysis constants and SIT coefficients. J. Chem. Thermodyn. 114, 2–13.
Anderson, J.S., 1969. Potassium polyuranates. Chimia 23, 438.
Baumann, A., Yalcintas, E., Gaona, X., Altmaier, M., Geckeis, H., 2017. Solubility and hydrolysis of Tc(IV) in dilute to concentrated KCl solutions: an extended

thermodynamic model for Tc^{4+}–H^+–K^+-Na^+–Mg^{2+}–Ca^{2+}-OH^-–Cl^-–H_2O(l) mixed systems. New J. Chem. 41, 9077–9086.
Berner, U.R., 1992. Thermodynamic modeling of cement degradation - impact of redox conditions on radionuclide release. Cement Concr. Res. 22, 465–475.
Brewitz, W., 1980. Programm zur Eignungsprüfung der Schachtanlage Konrad für die Einlagerung radioaktiver Abfälle-Zusammenfassender Zwischenbericht, GSF-T 114. Atomkernenergie-Kerntechnik, Braunschweig.
Bube, C., Metz, V., Bohnert, E., Garbev, K., Schild, D., Kienzler, B., 2013. Long–term cement corrosion in chloride–rich solutions relevant to radioactive waste disposal in rock salt – leaching experiments and thermodynamic simulations. Phys. Chem. Earth 64, 87–94.
Cevirim-Papaioannou, N., Yalcintas, E., Gaona, X., Dardenne, K., Altmaier, M., Geckeis, H., 2018. Redox chemistry of uranium in reducing, dilute to concentrated NaCl solutions. Appl. Geochem. https://doi.org/10.1016/j.apgeochem.2018.07.006.
Ciavatta, L., 1980. The specific interaction theory in evaluating ionic equilibria. Ann. Chim. 70, 551–567.
Diaz-Arocas, P., Grambow, B., 1998. Solid–liquid phase equilibria of U(VI) in NaCl solutions. Geochem. Cosmochim. Acta 62, 245–263.
Duro, L., Montoya, V., Colàs, E., García, A.B., 2010. Groundwater Equilibration and Radionuclide Solubility Calculations. Nuclear Waste Management Organization, Toronto, Canada.
Efremova, K.M., Ippolitova, E.A., Simanov, I.P., Spitsyn, V.I., 1959. An investigation of the composition of alkali element uranates obtained by a dry procedure. Dokl. Akad. Nauk SSSR 124, 1057–1060.
Endrizzi, F., Gaona, X., Marques Fernandes, M., Baeyens, B., Altmaier, M., 2018. Solubility and hydrolysis of U(VI) in 0.5 M NaCl solutions at T = 22 and 80°C. J. Chem. Thermodyn. 120, 45–53.
Frape, S.K., Fritz, P., Mcnutt, R.H., 1984. Water rock interaction and chemistry of groundwaters from the canadian shield. Geochem. Cosmochim. Acta 48, 1617–1627.
Frondel, J.W., Fleischer, M., 1954. Glossary of Uranium and Thorium-bearing Minerals. third ed. Geological Survey Bulletin 1009-F, USA Report.
Fuger, J., 1985. Thermochemistry of the alkali metal and alkaline earth-actinide complex oxides. J. Nucl. Mater. 130, 253–265.
Gaona, X., Fellhauer, D., Altmaier, M., 2013. Thermodynamic description of Np(VI) solubility, hydrolysis, and redox behavior in dilute to concentrated alkaline NaCl solutions. Pure Appl. Chem. 85, 2027–2049.
Gorman-Lewis, D., Burns, P.C., Fein, J.B., 2008a. Review of uranyl mineral solubility measurements. J. Chem. Thermodyn. 40, 335–352.
Gorman-Lewis, D., Fein, J.B., Burns, P.C., Szymanowski, J.E.S., Converse, J., 2008b. Solubility measurements of the uranyl oxide hydrate phases metaschoepite, compreignacite, Na–compreignacite, becquerelite, and clarkeite. J. Chem. Thermodyn. 40, 980–990.
Grenthe, I., Fuger, J., Konings, R.J.M., J, L.R., Müller, A.B., Nguyen-Trung, C., Wanner, H., 1992. Chemical thermodynamics of uranium. In: Vol. 1 of Chemical Thermodynamics. Elseiver Science Publishers, Amsterdam.
Grenthe, I., Drożdżyński, J., Fujino, T., Buck, E.C., Albrecht-Schmitt, T.E., Wolf, S.F., 2006. Uranium. In: Morss, L.R., Edelstein, N.M., Fuger, J. (Eds.), The Chemistry of the Actinide and Transactinide Elements. Springer, Dordrecht, pp. 253–698.
Guillaumont, R., Fanghänel, T., Fuger, J., Grenthe, I., Neck, V., Palmer, D.A., Rand, M.H., 2003. Update on the chemical thermodynamics of uranium, neptunium, plutonium, americium and technetium. In: Vol. 5 of Chemical Thermodynamics. Elseiver Science Publishers, Amsterdam.
Iyer, V.S., Jayanthi, K., Venugopal, V., 1997. Thermodynamic properties of $K_2U_4O_{12}$(s) and $K_2U_4O_{13}$(s) by EMF and calorimetric measurements. J. Solid State Chem. 132, 342–348.
JCPDS, 2001. Powder Diffraction Files. Joint Committee on Powder Diffraction Standards, Swarthmore, USA.
Jove, J., Cousson, A., 1988. Synthesis and crystal-structure of $K_2U_2O_7$ and mössbauer (Np-237) studies of $K_2Np_2O_7$ and $CaNpO_4$. J. Less Common. Met. 139, 345–350.
Kovba, L.M., 1970. Phase diagram of uranium-oxygen system. Dokl. Akad. Nauk SSSR 194, 98.
Kovba, L.M., 1972. $K_2U_7O_{22}$ crystalline structure. Zh. Strukt. Khim. 13, 256.
Kovba, L.M., Churbakova, T.I., 1961. X-Ray investigation of potassium polyuranates. Zh. Strukt. Khim. 2, 585–590.
Lucchini, J.F., Borkowski, M., Richmann, M.K., Ballard, S., Reed, D.T., 2007. Solubility of Nd^{3+} and $UO2^{2+}$ in WIPP brine as oxidation-state invariant analogs for plutonium. J. Alloy. Comp. 444, 506–511.
Nipruk, O.V., Chernorukov, N.G., Kostrova, E.L., Chernorukov, G.N., 2015. Synthesis and study of potassium uranates $K_2U_6O_{19}$ and $K_2U_4O_{13}\cdot 2.2H_2O$. Radiochemistry 57, 580–583.
Nipruk, O.V., Chernorukov, G.N., Abrazheev, R.V., Kostrova, E.L., 2017. Synthesis and characterization of sodium and potassium uranates with the compositions $Na_2[(UO_2)_6O_4(OH)_6]\cdot 8H_2O$ and $K_2[(UO_2)_6O_4(OH)_6]\cdot 8H_2O$. Inorganic Mater. 53, 816–819.
O'Hare, P.A.G., Hoekstra, H.R., 1974. Thermochemistry of uranium compounds V. standard enthalpies of formation of monouranates of lithium, potassium, and rubidium. J. Chem. Thermodyn. 6, 1161–1169.
Ochs, M., Dirk, M., Wang, L., 2016. Radionuclide and Metal Sorption on Cement and Concrete. Springer, Switzerland.
Saine, M.C., 1989. Synthesis and structure of monoclinic $K_2U_2O_7$. J. Less Common Mater. 154, 361–365.
Sandino, M.C.A., Grambow, B., 1994. Solubility equilibria in the U(VI)–Ca–K–Cl–H_2O system: transformation of schoepite into becquerelite and compreignacite. Radiochim. Acta 66 (7), 37–43.
Snider, A.C., 2003. Verification of the Definition of Generic Weep Brine and the Development of a Recipe for This Brine. Analysis Report. Sandia National Laboratories, Carlsbad, NM.
Taylor, H.F.W., 1997. Cement Chemistry, second ed. Thomas Telford, London.
Toussaint, C.J., Avogadro, A., 1974. Concerning uranate formation in alkali nitrate melts. J. Inorg. Nucl. Chem. 36, 781–784.
Van Egmond, A.B., Cordfunke, E.H.P., 1976. Investigations on potassium and rubidium uranates. J. Inorg. Nucl. Chem. 38, 2245–2247.
Wieland, E., Van Loon, L., 2003. Cementitious Near-field Sorption Data Base for Performance Assessment of an ILW Repository in Opalinus Clay. Technical Report. Paul Scherrer Institut, Villigen, Switzerland.
Yamazaki, H., Lagerman, B., Symeopoulos, V., Choppin, G.R., 1992. Solubility of uranyl in brine. Am. Soc. Civil Eng. 2, 1607–1611.